HHS Public Access

Author manuscript

*J Phys Chem B*. Author manuscript; available in PMC 2017 August 08.

Published in final edited form as:

*J Phys Chem B*. 2016 November 03; 120(43): 11180–11190. doi:10.1021/acs.jpcb.6b07119.

# Dynamics of Crowding-Induced Mixing in Phase Separated Lipid Bilayers

**Wade F. Zeno**[‡], **Kaitlin E. Johnson**[‡], **Darryl Y. Sasaki**[¶], **Subhash H. Risbud**[†], and **Marjorie L. Longo**[*,‡]

[‡]Department of Chemical Engineering, University of California Davis, Davis, California 95616, United States

[¶]Sandia National Laboratories, P.O. Box 969, Livermore, California 94551, United States

[†]Department of Materials Science and Engineering, University of California Davis, Davis, California 95616, United States

## Abstract

We use fluorescence microscopy to examine the dynamics of the crowding-induced mixing transition of liquid ordered ($L_o$)-liquid disordered ($L_d$) phase separated lipid bilayers when the following particles of increasing size bind to either the $L_o$ or $L_d$ phase: Ubiquitin, green fluorescent protein (GFP), and nanolipoprotein particles (NLPs) of two diameters. These proteinaceous particles contained histidine-tags, which were phase targeted by binding to iminodiacetic acid (IDA) head groups, via a $Cu^{2+}$ chelating mechanism, of lipids that specifically partition into either the $L_o$ phase or $L_d$ phase. The degree of steric pressure was controlled by varying the size of the bound particle (10-240 kDa) and the amount of binding sites present (i.e. DPIDA concentrations of 9 and 12 mol%) in the supported lipid multibilayer platform used here. We develop a mass transfer-based diffusional model to analyze the observed $L_o$ phase domain dissolution that, along with visual observations and activation energy calculations, provides insight into the sequence of events in crowding-induced mixing. Our results suggest that the degree of steric pressure and target phase influence not only the efficacy of steric-pressure induced mixing, but the rate and controlling mechanism for which it occurs.

## Graphical abstract

[*]Corresponding Author: mllongo@ucdavis.edu. Tel: 530-848-9340.

Supporting Information: The Supporting Information is available free of charge on the ACS Publications website. Detailed derivations, image processing, additional figures and tables.

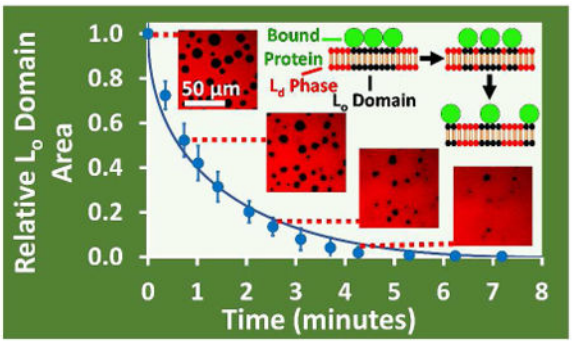


## Introduction

In aqueous environments, phospholipids self-assemble to form bilayers that can exist in either a solid or liquid phase.[1-4] Structure of the head group (i.e. size and charge), structure of the carbon tails (i.e. length and degrees of unsaturation), and temperature are several of the properties and conditions that determine whether a solid or liquid phase is formed.[2, 5] When an appropriate amount of cholesterol is added to a binary solid-liquid phospholipid mixture, the solid and liquid phases become liquid-ordered ($L_o$) and liquid-disordered ($L_d$) phases, respectively.[1-4] Fluorescent probes and functionalized lipids are capable of selectively partitioning into either of these coexisting, immiscible phases due to their distinct compositions.[6-7] The contrast from fluorescent probe partitioning allows for visualization of phase separation via fluorescence microscopy, while functionalized lipids can allow for targeted binding of proteins to specific phases. This type of phenomenon has been of interest for the development of a variety of biological materials, such as high-density arrays, microfluidic networks, and biosensors.[8-12] Tethering of proteins to bilayers via functionalized lipids has been previously achieved by several mechanisms, such as disulfide bonds, single-stranded DNA linkages, and biotinylation.[13-15] Another mechanism – the method of interest for the work presented here – is metal chelation.[16] Lipid head groups functionalized with iminodiacetic acid (IDA) are capable of coordinating divalent transition metals (e.g. $Zn^{2+}$, $Ni^{2+}$, $Cu^{2+}$) through four coordination sites, leaving the two remaining sites exposed.[17] Poly-histidine tags that are covalently attached to proteins of interest are then able to bind to these exposed sites. IDA membranes also exhibit reversibility after EDTA is added to the system, as EDTA sequesters metal ions, causing proteins to become unbound.[18-19]

Dipalmitoyl iminodiaceticacid (DPIDA) and dioleoyl iminodiaceticacid (DOIDA) are two IDA-functionalized lipids that have been used for phase targeting of histidine-tagged proteins. DPIDA has been demonstrated to partition into dipalmitoyl phosphocholine (DPPC)-rich $L_o$ phase, while DOIDA partitions into dioleoyl phosphocholine (DOPC)-rich $L_d$ phase when both phases are present in a bilayer.[20] This partitioning is due to similarities in carbon tail structures, degree of unsaturation, and length. Phase-specific binding of histidine-tagged proteins to DPIDA and DOIDA in the presence of Cu(II)has been extensively examined by Sasaki and coworkers.[18, 20-22] Histidine-tagged green fluorescent protein (GFP) was often used for studying targeted binding. When targeting DPIDA, GFP's

fluorescence served as a visual indicator of binding to the $L_o$ phase in $L_o$-$L_d$ phase separated unilamellar vesicles (GUVs). GUVs exhibited significant changes in shape and morphology, such as membrane bending and tubule formation. This was attributed to protein binding localized to the $L_o$ domains, which resulted in crowding in the headgroup region and induced local curvature. This was most often observed when diphytanoyl phosphocholine (DPhPC) was incorporated into GUVs.

Similarly, crowding-induced changes in $L_o$-$L_d$ phase separation in GUVs containing DPPC, DOPC, and cholesterol as the main constituents was examined by Scheve *et al.*[23] Targeting and binding of histidine-tagged Ubiquitin, GFP, and Transferrin to the $L_o$ phase was achieved via incorporation of DPIDA. Rather than membrane bending and tubule formation the percentage of GUVs that were phase separated decreased. This behavior was attributed to the large steric pressure localized to the $L_o$ domains by the $L_o$ phase-targeted binding that lead to mixing of the $L_o$ and $L_d$ phase lipids. There was also an obvious trend linking protein size to membrane mixing capacity as measured by the percentage of mixed GUVs. Phase separated lipid bilayers have an inherent free energy of mixing ($\Delta G_{mix}$),[24] thus Scheve *et al.* developed an empirical thermodynamic model to compare enthalpy of mixing to steric pressure exerted by bound proteins. Our previous work expanded upon the work of Scheve *et al.* to develop and experimentally test a first principles thermodynamic model that more universally describes mixing behavior and is capable of being used for a wide variety of lipid compositions.[25] The model consisted of a Boltzmann distribution that was applied to mixing within GUV populations (i.e. percentage of mixed and unmixed GUVs). It also incorporated the steric-pressure contribution to free energy via the Carnahan-Starling equation of state. Values for $\Delta G_{mix}$ were determined for various lipid compositions; its value decreased as a critical/mixing composition was approached, thus validating the thermodynamic model. Similarly to Scheve *et al.*, we reported an increase in mixing efficacy as the size of the particle binding to the $L_o$ phase of the GUV increased. We also qualitatively investigated $L_d$ phase targeting in GUVs via DOIDA incorporation and $L_o$ phase targeting in supported lipid multibilayers (MBLs) via DPIDA incorporation. In both instances mixing was observed at elevated IDA lipid concentration. Though the initial phase separated and final mixed states were analyzed, we made only a preliminary qualitative attempt to observe the kinetics and dynamics of the crowding-induced mixing process in one MBL sample.

In this present work, we utilize fluorescence microscopy to quantitatively examine the time-dependent crowding-induced mixing of $L_o$-$L_d$ phase separated lipid bilayers. The process was observed on supported lipid multibilayers consisting of DOPC/DPPC/cholesterol and DPIDA for $L_o$ targeting or DOIDA for $L_d$ targeting. Bilayers in a lipid multibilayer remain associated with a flat surface throughout the process of exchange of buffers yet distanced enough to be decoupled from strong interaction with the substrate, making it easy to follow the dynamics of individual domains over relatively long periods of time. We varied the steric pressure by varying the size and molecular weight of the histidine-tagged crowding agent and the surface density of the target lipid, DPIDA. A schematic of crowding-induced mixing in a phase-separated lipid bilayer, and its reversibility, is depicted in Fig. 1. Histidine-tagged Ubiquitin (2.5 nm diameter, 10 kDa) and GFP (3.6 nm diameter, 28 kDa) were used. In addition to this, two different sized populations of histidine-tagged nanolipoprotein particles

(NLPs) were used. NLPs are self-assembled particles consisting of phospholipids and proteins. Specifically, they are composed of a lipid bilayer patch (~100-200 lipids) with two parallel, amphiphilic membrane scaffold proteins (MSPs) belted around the outer periphery, shielding the exposed carbon lipid tails (Fig. 1). NLPs are discoidal in shape with a thickness of 5 nm (i.e. the thickness of a lipid bilayer), and a diameter that can vary on the order of 10-20 nm.[26] The diameter of an NLP population is controlled by the length of the MSP.[26-27] Histidine-tagged MSPs of various lengths are commercially available.[28-29] MSP1 (25 kDa) and MSP3 (33 kDa) were used to synthesize NLP1 (9 nm diameter, 140 kDa) and NLP3 (14 nm diameter, 240 kDa), respectively. Histidine-tagged NLPs are particularly useful for this work because of their large size scale and size tunability through our choice of the scaffold protein. Our previous work validated the use of NLPs as model crowding agents.[25] Here we show that particle size and target phase not only influences the efficacy of steric-pressure induced mixing, but the rate and controlling mechanism at which it occurs. We develop a mass transfer-based diffusional model that, along with visual observations and activation energy calculations, provides insight to crowding-induced mixing mechanisms.

## Materials and Methods

### Materials

Lyophilized, N-terminal histidine-tagged Ubiquitin was purchased from Sigma-Aldrich, Inc. Green fluorescent protein (GFP) also containing an N-terminal histidine-tag was purchased from Thermo Fisher Scientific. Lyophilized Membrane Scaffold Proteins (MSPs), which were used in the synthesis of NLPs, contained single N-terminal histidine tags and were purchased from Cube Biotech, Inc. The two types of MSP used were MSP1 (sold as MSP1D1-his, 217 amino acids, 25.3 kDa) and MSP3 (sold as MSP1E3D1-his, 277 amino acids, 32.6 kDa). Copper (II) chloride (≥ 99%), sodium cholate (≥ 99%), sodium chloride (≥ 99%), imidazole (≥ 99%), and methanol (≥ 99%) were purchased from Sigma-Aldrich, Inc. Chloroform was purchased from Fisher Scientific International, Inc. DPPC (1,2-dipalmitoyl-sn-glycero-3-phosphocholine), DOPC (1,2-dioleoyl-sn-glycero-3-phosphocholine), and cholesterol were purchased from Avanti Polar Lipids, Inc. Texas Red® DHPE (Texas Red® 1,2,-dihexadecanoyl-sn-glycero-3-phosphoethanolamine) and Oregon Green® 488 DHPE (Oregon Green® 488 1,2,-dihexadecanoyl-sn-glycero-3-phosphoethanolamine) were purchased in lyophilized states from Thermo Fisher Scientific. DPIDA[20] (1,2-dipalmitoyl-sn-glycero-triethyleneoxy-iminodiacetic acid) and DOIDA[30] (1,2-dioleoyl-sn-glycero-3-triethylenoxy-iminodiacetic acid) were synthesized according to previously reported protocols. Tris(hydroxymethyl)aminomethane [Tris] (MB Grade) and hydrochloric acid (12.1 N) were purchased from USB Corporation and Fisher Scientific International, Inc., respectively. Ni-NTA agarose was purchased from 5 PRIME, Inc. All water used in the work described was purified using a Barnstead Nanopure System (Barnstead Thermolyne, Dubuque, IA) with a minimum resistivity of 17.9 MΩ•cm.

### Preparation of Ubiquitin, GFP, and NLPs

Lyophilized Ubiquitin was dissolved in Tris Buffer (20 mM Tris, 100 mM NaCl, pH 7.4) at a concentration of 1 mg/mL then purified using Ni-NTA resin as described previously with other histidine-tagged proteins.[31-32] Protein yield was measured using UV-Vis absorption at

280 nm, then aliquoted and stored at -20°C. GFP was dissolved in water at a concentration of 0.1 mg/mL, aliquoted, and frozen at -20°C. Ubiquitin and GFP aliquots were thawed prior to binding experiments. NLPs containing DOPC and either MSP1 or MSP3 were synthesized exactly as previously described.[25] NLPs used for DPIDA binding experiments were doped with 0.1 mol% Oregon Green-DHPE, while NLPs used for DOIDA binding experiments were not. This was due to potential electrostatic repulsion between the Oregon Green-DHPE in NLPs and Texas-Red DHPE in the $L_d$ region of MBLs.[25]

## Lipid Multibilayer Binding and Imaging Experiments

Planar lipid multibilayers (MBLs) were prepared by a standard spin-coating technique as previously described.[25] Briefly, appropriate amounts of DOPC, DPPC, Cholesterol, DPIDA or DOIDA, and Texas Red-DHPE were combined, dried under nitrogen gas, and dissolved in a Hexane/Methanol solution (93 %v/v Hexane) at a concentration of 1.1 mg/mL total lipid. Samples were then spin-coated onto a 1 $cm^2$ mica substrate at 3000 RPM for 40 seconds and dried under vacuum for at least 2 hours. Samples were enclosed within open-top wells consisting of 3D printed polylactic acid (PLA) squares adhered to polystyrene Petri dishes with vacuum grease. PLA squares had dimensions of 1.5 cm × 1.5 cm with a depth of 0.4 cm. Each well was hydrated in Tris Buffer (20 mM Tris, 100 mM NaCl, pH 7.4), heated to 55°C on a heating plate, and held there for at least 5 minutes before being removed and allowed to cool to room temperature. After cooling, excess buffer around the outer periphery of the PLA well was removed. Prior to imaging, each well contained supported MBLs on mica hydrated with 900 μL of Tris buffer. To each well, 6.8 μL of 16 mM $CuCl_2$ was then added. Afterward, concentrated stocks of Ubiquitin, GFP, NLP1, or NLP3 were added to their respective sample such that the final concentration was 0.2 μM. After mixing behavior was observed, 3.6 μL of 0.5 M EDTA was added to remove proteins and observe domain reformation.

Imaging was performed using a 60× water immersion lens on a Nikon TE400 fluorescence microscope. The microscope contained FITC and Texas Red filters (Chroma Technology, Bellows Falls, VT). For visualization of GFP and Oregon Green-DHPE-containing NLPs, the FITC filter was used, while Texas Red Filters were used to visualize MBLs containing Texas Red-DHPE. Since Ubiquitin is non-fluorescent, it could not be visualized directly. With the concentrations of dye and protein used, no visual overlap was observed between the two filters (i.e. lipid domains could not be seen in the FITC filter and GFP/NLPs could not be seen in the Texas-Red Filter).

## Data Processing and Numerical Methods

Microscope images of MBLs used in quantitative analysis for examining diffusion behavior were processed by converting 16-bit images to black/white binary pixelated images with ImageJ as shown in Fig. S3. The area fractions of the converted images were then determined using the “Analyze Particles” tool. Standard deviations of 4 quadrants within the microscope field of view were used to determine the error in Area Fraction for data points that were regressed. Processed images were regressed with Least Squares using the Runge-Kutta $4^{th}$ order method for numerical integration. The program for finding numerical solutions was written and performed in MATLAB. Errors in regressed parameters were

determined by regressing parameters to the upper and lower ends of error bars from experimental data.

## Results

### Dynamics of Steric Pressure-Induced Mixing by Binding to $L_o$ Phase

We incubated histidine-tagged Ubiquitin (~10 kDa), GFP (~28 kDa), NLP1 (~140 kDa), or NLP3 (~240 kDa) with supported lipid multibilayers (MBLs) that contained two different concentrations of DPIDA, 12 mol% or 9 mol% in a 3:2 molar ratio of DOPC:(DPPC +DPIDA), 18 mol% cholesterol, and 0.1 mol% Texas Red-DHPE. These compositions display liquid ordered ($L_o$) - liquid disordered ($L_d$) phase coexistence.[23] The DPIDA lipid partitions to the $L_o$ phase and the histidine tags of proteins bind to the IDA headgroup in the presence of Cu(II), thus targeting binding to the $L_o$ phase.[20, 23] Texas Red-DHPE partitions strongly to the $L_d$ phase such that the $L_o$ phase domains appear dark by fluorescence microscopy as shown in Fig. 2A. Cohen-Simonsen and coworkers have shown that the $L_o$ phase domains proximal to the substrate are sub-microscopic while those in subsequent bilayers coarsen quickly to form microscopic domains, as seen in Fig 2A.[33] The domains observed here are in the second, and only other, bilayer distal to the substrate indicated by the lack of observation of any overlapping domains.

We observed crowding-induced dissolution of the $L_o$ domains of MBLs containing 12% DPIDA when incubated with histidine-tagged GFP, NLP1, and NLP3, as demonstrated by a decrease in domain size as time progressed in Fig. 2A-D. We characterize the dynamics of this crowding-induced mixing mechanism by plotting the relative $L_o$ domain Area Fractions (AF), i.e. $AF/AF_{0,}$ vs. time, which decays exponentially to zero (apparently complete dissolution) as shown in Fig. 3A. The $L_o$ domains bound by the smallest species, Ubiquitin, exhibited partial dissolution with a final relative AF of 0.87±0.08, but no clear exponential decay (Fig. 3A). The $L_o$ domains bound by GFP, NLP1, and NLP3, in order of smallest to largest, exhibited a final relative AF of zero within 9, 6, and 2 minutes, respectively. Immediately afterward, 2 mM EDTA was used to remove these bound proteins, resulting in the reappearance and growth of $L_o$ domains as demonstrated in Fig 2D-F. In Fig. 3B, it can be seen that the relative AF returned to 80% of the original value for GFP and 90% for NLP1 and NLP3 within 1 minute after EDTA is added, indicating that the dissolution that we observe here is a reversible mixing transition. During all domain dissolution and domain growth, the vicinity close to the domains tended to have a granular appearance as shown clearly in Fig. 2B (inset).

For MBLs containing 9 mol% DPIDA, complete dissolution of the $L_o$ domains was observed when incubated with NLP3, the largest species of the four (Fig. 3C). Incubation with NLP1 resulted in significant dissolution, with a residual relative AF of 0.06±0.01 after completion. This final value did not change significantly over the final 5 minutes as seen with the data points in Fig. 3C. After addition of 2 mM EDTA, the relative AF for these two cases returned to 85-90% of their original value within a 1 minute time period, as shown in Fig. 3D. No significant change in relative AF was observed when incubating in the smaller species, Ubiquitin or GFP, over an 8-9 minute period as shown in Fig. 3C.

Dissolution of $L_o$ phase domains began immediately after NLP1 and NLP3 were added to phase-separated MBLs containing 12 mol% DPIDA and when the larger of the two NLPs, NLP3, was added to phase-separated MBLS containing 9 mol% DPIDA. However, for other samples, immediately after protein was added, smaller $L_o$ domains were ejected from larger $L_o$ domains, keeping the relative AF constant over the course of about 1 minute as demonstrated in Fig. 4A-B. These ejected domains were seen to grow by coalescence or Ostwald ripening as demonstrated in Fig. 4B-C. Imaging of bound GFP showed that the bound species were primarily located in the $L_o$ phase (small and large green domains in Fig. 4C) during this initial period. After this initial period of domain break up, domains proceeded to dissolve for GFP binding (demonstrated in Figs. 4D-F in Texas Red channel and Fig. S4 for representative GFP channel images) or Ubiquitin binding to 12 mol% DPIDA MBLs and NLP1 binding to 9 mol% DPIDA MBLs. In the case of Ubiquitin binding to 12 mol% DPIDA MBLs, domain dissolution took place so slowly that coalescence and Ostwald ripening were still observable phenomena during dissolution (see Fig. S5). Only the domain break-up was observed when GFP was incubated with 9 mol% DPIDA MBLs. The small protein Ubiquitin imparted no observable change in relative AF or domain size to the 9 mol% DPIDA MBLs.

## Modeling of Steric Pressure-Induced $L_o$ Domain Dissolution and Curve Fitting

The dissolution of liquid ordered domains was modeled using the time-dependent diffusion equation, as shown in equation 1, where D corresponds to the diffusivity of the lipids ($\mu m^2/s$). The idealized system is illustrated in Fig. 5A, where $L_o$ domains are shown starting with an initial radius of $R_o$ that decreases in size over time. The region of mass transfer (r) corresponds to the annulus between the outer periphery of a domain (R(t)) and the average midpoint to neighboring domains ($R_b$). $R_o$ corresponds to the average initial domain radius. The initial and boundary conditions for equation 1 are listed in equations 1a-c. At initial time, there is a concentration of $L_o$ domain lipids in the annulus ($C_1$). The $L_o$ domains are assumed to have constant, uniform concentrations of $C_o$ throughout the dissolution process. Since domain lipids diffuse outwardly towards the boundaries, the net flux across boundaries midway between domains is equal to zero.

$$\frac{\partial c(t,r)}{\partial t} = D\nabla^2 C(t,r), \quad t \in [0,\infty], \quad r \in [R(t), R_b] \quad (1)$$

$$C(0,r) = C_1 \quad (1a)$$

$$C(t,R) = C_o \quad (1b)$$

$$\frac{\partial C}{\partial r}\Big|_{r=R_b}=0 \quad (1c)$$

Equation 1 was solved analytically using separation of variables and a 1-dimensional Cartesian Laplacian (Fig. 5B), rather than cylindrical, because an analytical solution in cylindrical coordinates with the given boundary conditions is difficult to obtain. By looking at numerical solutions to both Cartesian and Cylindrical coordinates, it was found that this is a reasonable approximation in the region of the concentration profile close to the domain boundary (i.e. the region of interest for this analysis). The concentration profile is shown in equation 2, where the eigenvalues of the Sturm-Liouville problem are defined in equation 2a. (See Supporting Information for detailed derivation)

$$C(t,r)\approx C_o+2C_o\left(\frac{C_1}{C_o}-1\right)\sum_{n=0}^{\infty}\left[e^{-\frac{\lambda_n^2 Dt}{(R_b-R)^2}}\sin\left(\frac{\lambda_n(r-R)}{R_b-R}\right)\left(\frac{1}{\lambda_n}\right)\right] \quad (2)$$

$$\lambda_n=\pi\left(\frac{2n+1}{2}\right) \quad (2a)$$

An interfacial mass balance was performed around the outer surface of a domain. The time-dependent rate of change of mass within a domain is equal to the flux of lipids out of the domain multiplied by the domain perimeter. The ordinary differential equation for this balance is shown in equation 3, with an initial condition of the radius equal to $R_o$ (equation 3a).

$$\frac{d}{dt}[C_o\pi R(t)^2]=D\frac{\partial C}{\partial r}\Big|_{r=R(t)}[2\pi R(t)] \quad (3)$$

$$R(0)=R_o \quad (3a)$$

By algebraically manipulating equation 3 and substituting in equation 2 for C, equation 4 for $\frac{dR}{dt}$ was obtained and solved numerically. The average relative area ($R/R_o$) of domains corresponds to the relative area fraction ($AF/AF_0$) as shown in equation 5.

$$\frac{dR}{dt}=\frac{2D\left(\frac{C_1}{C_o}-1\right)}{(R_b-R)}\sum_{n=0}^{\infty}\left[e^{-\frac{\lambda_n^2 Dt}{(R_b-R)^2}}\right] \quad (4)$$

$$\frac{\mathrm{AF}}{\mathrm{AF}_o}=\left(\frac{R}{R_o}\right)^2 \quad (5)$$

The data for $AF/AF_0$ vs. time in Fig. 3A and Fig. 3C were regressed using equations 4 and 5 by the least squares method. The variable parameters for this regression were D and $C_1/C_o$. For modelling the reversed process (i.e. protein removal and domain reformation), equations 4 and 5 were used with a negative sign on the right hand sign of equation 4, as the diffusive flux is now into the domain rather than out of it. The value of $AF_0$ from the mixing model was used for its corresponding reversal model.

As shown in Fig. 3, regression curves are in agreement with experimental data, for all samples. Meaningful regression curves could not be generated in the cases where there was no dissolution or where the change in relative AF was minor. Diffusion coefficients (D) obtained from dissolution data appear to be correlated to the size of the bound protein or NLP, as seen in Table 1. D increased from ~0.02 $\mu m^2/s$ to an at least an order of magnitude higher as particle size increased from 10 $nm^2$ (GFP) to 153 $nm^2$ (NLP3). It is also worth noting that bound NLP3 imparted a higher D value in 12 mol% DPIDA in comparison to 9 mol% DPIDA. Diffusion coefficients obtained by demixing data shown in Table 1 were of magnitude ~0.5 $\mu m^2/s$, and relatively similar for all samples, as expected, since protein was no longer bound.

## Activation Energy Approximation for Steric Pressure-Induced $L_o$ Domain Dissolution

The range of diffusion coefficients obtained from the dissolution data could indicate a transition from a kinetically-limited process (slow dissolution) to a diffusion-limited process (fast dissolution). The activation energy ($E_A$) associated with lipids transferring from a $L_o$ domain to the surrounding $L_d$ region was approximated using Arrhenius kinetics. Detailed calculations are provided in the Supporting Information. Briefly, relative rates of domain dissolution induced by GFP, NLP1, and NLP3 binding to 12 mol% DPIDA MBLs were compared. Using the Arrhenius equation (equation 6), an activation energy cannot be calculated directly since there are 3 equations (an Arrhenius equation for each particle binding) and 4 unknowns (an Activation Energy for each particle binding and the Arrhenius pre-exponential factor A).

$$\text{reaction rate} \propto k = Ae^{-\frac{E_A}{k_B T}} \quad (6)$$

By comparing regressed first-order reaction rate constants (k) between two samples, a change in activation energy $\Delta E_A$ was determined. Dissolution time scales decreased as particle size increased (Fig. 3), indicating that $E_A$ also decreased as particle size increased (i.e. reaction rate increased). MBLs bound with NLP1 exhibited a 0.1kT decrease in $E_A$ relative to MBLs bound with GFP, whereas MBLs bound with NLP3 exhibited 1.8kT decrease in comparison to those bound with NLP1. Based on these values for $\Delta E_A$, we were able to infer that $E_A$ for a bilayer with no particles bound is on the order of 1-2kT (~ 4 to $8\times10^{-21}$ Joules/lipid).

### Determination of $\Delta G_{mix}$ from Steric Pressure-Induced $L_o$ Domain Dissolution

The Boltzmann distribution, shown in equation 7, relates the free energy to the partitioning of lipids between two states (mixed and unmixed) at equilibrium.[34] For the system being examined, there are two contributions to the free energy; the inherent free energy of mixing ($\Delta G_{mix}$) and the free energy associated with steric pressure ($\Delta G_p$). The partition coefficient (K) is shown in equation 7 and defined in equation 8 as the ratio of unmixed lipids to mixed lipids at equilibrium. This result was obtained by performing a mass balance on a domain with initial and final equilibrium radii assuming a mixing zone exists. (See supporting information).

$$k_B T * \ln(K) = \Delta G_{\mathrm{mix}} + \Delta G_p \quad (7)$$

$$K = \frac{N_{\mathrm{unmixed}}}{N_{\mathrm{mixed}}} = \frac{\frac{1}{\mathrm{AF}_o} - \left(1 - \frac{\mathrm{AF}}{\mathrm{AF}_o}\right)\left(\frac{1}{\mathrm{AF}_o} - \frac{\mathrm{AF}}{\mathrm{AF}_o}\right)}{\left(1 - \frac{\mathrm{AF}}{\mathrm{AF}_o}\right)\left(\frac{1}{\mathrm{AF}_o} - \frac{\mathrm{AF}}{\mathrm{AF}_o}\right)} \quad (8)$$

Previously, we demonstrated that the steric pressure contribution to free energy can be determined by integrating the Carnahan-Starling equation state over the change in fractional surface coverage ($\eta$) of the binding species before and after complete mixing.[25] The initial surface coverage ($\eta_i$) and final surface coverage ($\eta_f$) were determined by knowing how much DPIDA is contained in the bilayer.[23, 25] We did not include an additional term for electrostatic interactions because the Debye length is short (~0.5 nm) in the presence of electrolytes. Details of these calculations are provided in the Supporting Information. When this is applied to $\Delta G_p$ in equation 7, equation 9 is obtained. $N_P$ and $N_L$ correspond to the number of proteins and lipids in a given area of bilayer, respectively.

$$\Delta G_{\mathrm{mix}} k_B T * \ln(K) - \int_{\eta_i}^{\eta_f} \frac{N_p}{N_L} k_B T \left(\frac{1+\eta+\eta^2-\eta^3}{\eta[1-\eta]^3}\right) d\eta \quad (9)$$

Use of equation 9 requires a final relative AF that is neither 0 nor 1. Two samples yielded values that satisfy this criteria; NLP1 bound to 9 mol% DPIDA MBLs (0.06 ± 0.01) and

Ubiquitin bound to 12 mol% DPIDA MBLs (0.87 ± 0.08). Based on these AF values, $\Delta G_{mix}$ was determined to be (1.0±0.5) × $10^{-20}$ Joules/Lipid for the former, and (1.1±0.3) × $10^{-20}$ Joules/Lipid for the latter. These values are on the same order of magnitude as those previously determined for this lipid composition in giant unilamellar vesicles.[25]

## Steric Pressure-Induced Membrane Remodeling by Binding to $L_d$ Phase

Next, we incubated histidine-tagged NLP1 (~140 kDa) with lipid multibilayers (MBLs) of compositions that display liquid ordered ($L_o$) - liquid disordered ($L_d$) phase coexistence and contained 20 mol% DOIDA, 18 mol% cholesterol, 0.1 mol% Texas Red-DHPE, and a 3:2 molar ratio of DOPC:(DPPC+DPIDA). The DOIDA lipid partitions to the $L_d$ phase, therefore histidine-tagged NLP1 binds primarily to the $L_d$ domains rather than the $L_o$ domains. As shown in Figs. 6A-C, binding of NLP1 to the $L_d$ region resulted in a generally less circular appearance of the $L_o$ domains, some of which appear to have coalesced. The relative AF of the domains had not perceptively changed. However, small, light $L_d$ domains can be seen to appear inside the $L_o$ domains after 1.5 minutes (Fig. 6C). This phenomenon is similar to the break-up of the $L_o$ phase observed previously for example in Fig. 4A-C. The $L_d$ region also appeared to darken as time progressed. After addition of 2 mM EDTA (Figs. 6D-F), the $L_d$ region became brighter and numerous small vesicles appeared on the edges of the $L_o$ domains, as indicated by the white dots, and the domains took on a leaf-like shape as seen in Fig. 6D. In addition, holes formed in the $L_d$ portion of the bilayer as illustrated by the irregularly shaped dark red patches. $L_o$ domains proceeded to become more round and coalesce while avoiding contact with bilayer holes, while entrapping some $L_d$ “subdomains” within the $L_o$ domains (Fig. 6D-E).

When we waited longer before adding the EDTA, the $L_d$ domains inside of the $L_o$ domains appear to increase in density and finally form vesicles (see Fig. S6) rather than mixing with the $L_o$ phase via dissolution. Therefore, the quantitative dissolution model could not be applied to these binding experiments. Wide-spread removal of the MBL through a process reminiscent of surface folding was the next step (Data not shown). When EDTA was added no reversible effects were observed.

The elongated appearance and lack of change in size of the domains was initially thought to be indicative of a gradual mixing process, akin to reversal of spinodal decomposition. To investigate this hypothesis, domain formation during cooling at this same lipid composition was observed as shown in Fig. 7. The domain formation is clearly indicative of nucleation and growth with the lipid composition used, thus the observed behavior is likely not related to spinodal decomposition.

## Steric Pressure-Induced Mixing by Binding to $L_o$ Phase in the Spinodal Region

To further examine the possibility that the mechanism of the mixing process is coupled with the mechanism of domain formation (i.e. nucleation and growth vs. spinodal decomposition), we examined the targeted binding of NLP1 to $L_o$ domains in MBLs with a composition consisting of a 1:1 DOPC:(DPPC+DPIDA) with 26 mol% Cholesterol and 0.1 mol% Texas Red-DHPE. The DPIDA concentration used was 14 mol%. In Fig. 8, it can be seen that this composition was in the spinodal region of the phase diagram indicated by the

elongated interlaced domain shapes (Fig. 8B) during domain formation by cooling. After $L_o$ domain formation and NLP1 addition to the system, domains were observed to undergo mixing via dissolution over the course of 3 minutes as illustrated in Figs. 9A-D. Upon removal of the NLP1 with EDTA (Figs. 9E-F), $L_o$ domains reappeared and were elongated enough (Fig. 8C and Fig. 9E are comparable) to suggest recovery of growth in the spinodal region. These results indicate that during $L_o$ targeted mixing of MBLs, the domains will undergo mixing via a dissolution mechanism rather than gradual spinodal-like mixing regardless of their compositional location on a phase diagram.

## Discussion

Crowding-induced dissolution of $L_o$ phase domains in $L_o$-$L_d$ phase separated lipid bilayers could involve two sequential rate processes, the kinetic process of release of $L_o$ phase clusters from the domains followed by diffusion of those clusters driven by a concentration gradient. Evidence includes the increase by almost 2 orders of magnitude in the diffusion coefficients calculated from the dissolution data as the steric pressure is increased by increasing the size of the bound protein or NLP. In comparison there is a relatively steady diffusion coefficient calculated from the time-dependent growth of domains after removal of the bound proteins or NLPs by EDTA. The variation in this apparent diffusion coefficient could represent a transition from a slow kinetically-limited dissolution process at low steric pressure, induced by a small bound protein such as GFP, to faster kinetics and thus a diffusion-limited process at high steric pressure, induced by a large bound particle such as NLP3. This could be explained by considering the mechanism of the kinetic process. The intermediate state is likely a thermal shape fluctuation of the domain boundary that results in pinching off of a small cluster of the target phase evidenced by the graininess, i.e. domains below ~0.5 μm in size, in the $L_d$ regions surrounding domains as they dissolved. Such thermal fluctuations are normally of energy approximately kT.[34] As the size of the bound particle increases, the free energy contribution from steric pressure is increased. This corresponds to higher energy in the initial, phase-separated state. This relative increase in initial energy would result in a decrease of the energy barrier for the mixing process. Using Arrhenius kinetics, this corresponds to a faster rate of reaction, i.e. pinching off clusters, as steric pressure is increased. Thus this kinetic process would no longer limit the dissolution rate. We calculated that the decrease in the activation energy would have to be at least 1.8 kT in agreement the energy scale of commonly occurring thermal shape fluctuations.

The plateau in diffusion coefficient values between 0.2 $\mu m^2/s$ and 0.8 $\mu m^2/s$ is additional evidence of dissolution (and regrowth) by lipid clusters vs individual lipids, as diffusivity generally varies inversely with cluster size. Typical diffusion coefficients for lipids diffusing in an $L_d$ phase are on the order of 1-10 $\mu m^2/s$.[35-37] The Saffman–Delbrück model is an appropriate model for calculating diffusion coefficients of species within lipid bilayers.[38] Using this model, it was calculated that lipid clusters consisting of $10^3$-$10^4$ lipids result in an order of magnitude reduction of diffusion coefficient relative to that of a single lipid (see Supporting Information). Clusters of such small size would only appear as a change in image texture (graininess) of the region around the dissolving or regrowing domains – consistent with what is observed. Such nanoscopic clusters are capable of dissolving or appearing rapidly through thermal compositional fluctuations which we postulate happened

in the final stage of mixing by the highest free energy contributions from steric pressure (NLP3 bound to 9 mol% and 12 mol% DPIDA domains and NLP1 bound to 12 mol% DPIDA domains) and first stage of regrowth by addition of EDTA.

We attempted to change the mechanism of crowding-induced mixing from dissolution (reversal of nucleation and growth) to gradual demixing (reversal of spinodal decomposition) by changing the membrane composition to one that is near a critical point. However, dissolution was still observed in the new composition when NLP1 bound to the $L_o$ phase. This can be explained by considering that during domain formation, small composition fluctuations in the spinodal region of the phase diagram exhibit negative free energies, thus making them favorable.[39] This allows for the gradual formation of interlaced domains that gradually change in composition, as typically seen in spinodal decomposition. However, when the process is reversed (i.e. steric pressure induced mixing), the composition fluctuations now exhibit positive free energies and are unfavorable. This eliminates the gradual mixing of the two phases as a process. It becomes more favorable to maintain the initial compositions of the $L_d$ and $L_o$ phases during mixing process as this minimizes composition fluctuations. The dissolution process occurring via lipid clusters rather than individual lipids is especially favorable, since they help to maintain domain composition. These can finally break up through large compositional fluctuations similar to reversal of nucleation.

When the magnitude of the free energy contribution from the crowding pressure ($\Delta G_{p,}$ a negative number) is less than the free energy change from mixing ($\Delta G_{mix}$), the addition of $\Delta G_p$ to $\Delta G_{mix}$ gives a new apparent $\Delta G$. This smaller $\Delta G$ will, in turn, be associated with a new equilibrium composition of each phase with more similar compositions closer to a critical point. A possible mechanism to achieve this new equilibrium was observed here in the break-up of the target phase by release of micron-scale domains from the target phase. The similarity in size of the ejected domains is suggestive of a Plateau-Raleigh line tension-driven instability which would be interesting to characterize using high-speed microscopy equipment in the future. The release of small domains of the target phase was followed by Ostwald ripening and coalescence as these may serve as mechanisms to move to a new equilibrium composition of each phase by slightly readjusting the composition of each phase without significantly changing the relative area fraction of each phase. In case the new equilibrium compositions nearly merge, i.e. near a critical point, the line tension is extremely low which may contribute to the stabilization of submicroscopic domains.[40] This might be mistaken as complete mixing when in fact nanoscopic domains still exist. This might explain the apparent observation of complete dissolution of $L_o$ domains in MBLs containing 12 mol% DPIDA when bound by GFP, as this was not expected. The calculated free energy contribution from steric pressure ($\Delta G_p$) for GFP binding to 12 mol% DPIDA MBLs was $-5.5 \times 10^{-21}$ Joules/Lipid, as determined from the integral term in equation 9. The magnitude of $\Delta G_p$ is smaller than $\Delta G_{mix}$ determined to be roughly $(1.0 \pm 0.5) \times 10^{-20}$ Joules/Lipid.

When targeting the crowding agent, NLP1, to the $L_d$ phase, membrane shape changes such as vesiculation and hole formation, played a major role in the drive toward equilibrium making it difficult to study mixing. Although we did find some evidence of lipid mixing,

(i.e. the appearance of micron-scale $L_d$ domains in the $L_o$ phase domains), it is interesting that a similar experiment resulted in complete mixing of approximately 80% of the population of GUVs in our previous work.[25] This could be accounted for by a difference in tension of the bilayers used in these two studies. MBLs are presumably free of any osmotic gradients that would create tension to smooth out membrane bending. The GUVs in our previous study were placed in a slightly hypotonic solution that creates enough tension to prevent excessive vesiculation.

## Conclusions

We examined the lipid mixing and demixing dynamics in $L_o$-$L_d$ phase separated supported lipid multibilayers induced by steric pressure from phase targeted binding of histidine-tagged proteins and molecular assemblies of various sizes. When targeting the $L_o$ phase by inclusion of DPIDA, mixing by the process of $L_o$ domain dissolution was suggestive of a two-step reaction-diffusion process, reaction-limited and slow when the steric pressure was low and diffusion-limited and fast when steric pressure was sufficiently high. Visual observation and the scale of the diffusion coefficients, determined through mass transfer analysis of the data, indicate that $L_o$ domains appeared to break up and dissolve into the neighboring phase via ejection of sub-microscopic clusters and/or micron-scale domains rather than individual lipids. Therefore, the initial reaction consisted of release of lipid clusters from $L_o$ domains via shape fluctuations of the domain perimeter that we determined were of energetic order kT. This was followed by diffusion of lipid clusters via a concentration gradient in the $L_d$ region. Reversibility was exhibited in all instances where domains appeared to completely or nearly completely dissolve. These results were obtained by targeting $L_o$ domains that formed in the nucleation and growth region of the phase diagram. For $L_o$ domains formed in the spinodal region of the phase diagram, $L_o$ domains mixed in a manner nearly identical to the dissolution observed in the nucleation and growth region as demanded by the curvature of the mixing energy with respect to composition. Moreover, using theory we previously derived, we were able to calculate values of $\Delta G_{mix}$ for lipid multibilayers that are in agreement with our previously reported values for giant unilamellar vesicles using similar compositions. In addition to $L_o$ domain targeting and dissolution, we qualitatively examined $L_d$ region targeting in MBLs using DOIDA. We found that the overall mixing process induced by steric pressure from the $L_d$ phase is inherently more complex and differs from what was observed with $L_o$ targeting, as the $L_d$ phase is more prone to deformation and shape fluctuations out of the two-dimensional MBL plane.

## Supplementary Material

Refer to Web version on PubMed Central for supplementary material.

## Acknowledgments

MLL, SHR, WFZ, and KEJ acknowledge partial support from the National Science Foundation under award number DMR-1500275. WFZ was partially supported by Grant Number T32-GM008799 from NIGMS-NIH. SHR also acknowledges partial support derived from his Blacutt-Underwood Endowed Chair funds. DYS was supported by the US Department of Energy, Office of Basic Energy Sciences, Division of Materials Science and Engineering. Sandia National Laboratories is a multi-program laboratory managed and operated by Sandia Corporation, a wholly

owned subsidiary of Lockheed Martin Corporation, for the U.S. Department of Energy's National Nuclear Security Administration under contract DE-AC04-94AL85000.

## References

1. Marsh D. Cholesterol-Induced Fluid Membrane Domains: A Compendium of Lipid-Raft Ternary Phase Diagrams. Biochim Biophys Acta. 2009; 1788:2114–2123. [PubMed: 19699712]
2. Veatch SL, Keller SL. Seeing Spots: Complex Phase Behavior in Simple Membranes. Biochim Biophys Acta. 2005; 1746:172–185. [PubMed: 16043244]
3. Juhasz J, Sharom FJ, Davis JH. Quantitative Characterization of Coexisting Phases in DOPC/DPPC/Cholesterol Mixtures: Comparing Confocal Fluorescence Microscopy and Deuterium Nuclear Magnetic Resonance. Biochim Biophys Acta. 2009; 1788:2541–2552. [PubMed: 19837045]
4. Lingwood D, Simons K. Lipid Rafts as a Membrane-Organizing Principle. Science (Washington, DC, U S). 2010; 327:46–50.
5. Rawicz W, Olbrich KC, McIntosh T, Needham D, Evans E. Effect of Chain Length and Unsaturation on Elasticity of Lipid Bilayers. Biophys J. 2000; 79:328–339. [PubMed: 10866959]
6. Juhasz J, Davis JH, Sharom FJ. Fluorescent Probe Partitioning in Guvs of Binary Phospholipid Mixtures: Implications for Interpreting Phase Behavior. Biochim Biophys Acta. 2010; 1818:19–26.
7. Momin N, Lee S, Gadok A, Busch D, Bachand G, Hayden C, Stachowiak J, Sasaki DY. Designing Lipids for Selective Partitioning into Liquid Ordered Membrane Domains. Soft Matter. 2015; 11:3241–3250. [PubMed: 25772372]
8. Bally M, Bailey K, Sugihara K, Grieshaber D, Voros J, Stadler B. Liposome and Lipid Bilayer Arrays Towards Biosensing Applications. Small. 2010; 6:2481–2497. [PubMed: 20925039]
9. Cornell BA, Breach-Maksvytis VLB, King LG, Osman PDJ, Raguse B, Weieczorek L, Pace RJ. A Biosensor that Uses Ion Channel Switches. Nature (London, U K). 1997; 387:580–582. [PubMed: 9177344]
10. Stelzle M, Weissmüller G, Sackmann E. On the Application of Supported Bilayers as Receptive Layers for Biosensors with Electrical Detection. J Phys Chem. 1993; 97:2974–2981.
11. Ogunyankin MO, Longo ML. Metastability in Pixelation Patterns of Coexisting Fluid Lipid Bilayer Phases Imposed by E-Beam Patterned Substrates. Soft matter. 2013; 9:2037–2046. [PubMed: 23483871]
12. Karlsson M, Sott K, Cans AS, Karlsson A, Karlsson R, Orwar O. Micropipette-Assisted Formation of Microscopic Networks for Unilamellar Lipid Bilayer Nanotubes and Containers. Langmuir. 2001; 17:6754–6758.
13. Seitz M, Wong JY, Park CK, Alcantar NA, Israelachvili J. Formation of Tethered Supported Bilayers Via Membrane-Inserting Lipids. Thin Solid Films. 1998; 327:767–771.
14. Svedhem S, Pfeiffer I, Larsson C, Wingren C, Borrebaeck C, Hook F. Patterns of DNA-Labeled and scFv-Antibody-Carrying Lipid Vesicles Directed by Material-Specific Immobilization of DNA and Supported Lipid Bilayer Formation on $Au/SiO_2$ Template. ChemBioChem. 2003; 4:339–343. [PubMed: 12672114]
15. Darst SA, Ahlers M, Meller PH, Kubalek EW, Blankenburg R, Ribi HO, Ringsdorf H, Kornberg RD. 2-Dimensional Crystals of Strepavidin on Biotinylated Lipid Bilayers and their Interactions with Biotinylated Macromolecules. Biophys J. 1991; 59:387–396. [PubMed: 1901232]
16. Nye JA, Groves JT. Kinetic Control of Histidine-Tagged Protein Surface Density on Supported Lipid Bilayers. Langmuir. 2008; 24:4145–4149. [PubMed: 18303929]
17. Bornhorst JA, Falke JJ. Purifcation of Proteins Using Polyhistidine Affinity Tags. Methods Enzymol. 2000; 326:245. [PubMed: 11036646]
18. Hayden CC, Hwang JS, Abate EA, Kent MS, Sasaki DY. Directed Formation of Lipid Membrane Microdomains as High Affinity Sites for His-Tagged Proteins. J Am Chem Soc. 2009; 131:8728–8729. [PubMed: 19505102]
19. Ng K, Pack DW, Sasaki DY, Arnold FH. Engineering Protein-Lipid Interactions: Targeting of Histidine-Tagged Proteins to Metal-Chelating Lipid Monolayers. Langmuir. 1995; 11:4048–4055.

20. Stachowiak JC, Hayden CC, Sanchez MAA, Wang J, Bunker BC, Voigt JA, Sasaki DY. Targeting Proteins to Liquid-Ordered Domains in Lipid Membranes. Langmuir. 2010; 27:1457–1462. [PubMed: 21155607]
21. Stachowiak JC, Hayden CC, Sasaki DY. Steric Confinement of Proteins on Lipid Membranes can Drive Curvature and Tubulation. Proc Natl Acad Sci U S A. 2010; 107:7781–7786. [PubMed: 20385839]
22. Stachowiak JC, Schmid EM, Ryan CJ, Ann HS, Sasaki DY, Sherman MB, Geissler PL, Fletcher DA, Hayden CC. Membrane Bending by Protein-Protein Crowding. Nat Cell Biol. 2012; 14:944–949. [PubMed: 22902598]
23. Scheve CS, Gonzales PA, Momin N, Stachowiak JC. Steric Pressure between Membrane-Bound Proteins Opposes Lipid Phase Separation. J Am Chem Soc. 2013; 135:1185–1188. [PubMed: 23321000]
24. Almeida PF. Thermodynamics of Lipid Interactions in Complex Bilayers. Biochim Biophys Acta. 2009; 1788:72–85. [PubMed: 18775410]
25. Zeno WF, Rystov A, Sasaki DY, Risbud SH, Longo ML. Crowding-Induced Mixing Behavior of Lipid Bilayers: Examination of Mixing Energy, Phase, Packing Geometry, and Reversibility. Langmuir. 2016; 32:4688–4697. [PubMed: 27096947]
26. Bricarello DA, Smilowitz JT, Zivkovic AM, German JB, Parikh AN. Reconstituted Lipoprotein: A Versatile Class of Biologically-Inspired Nanostructures. ACS Nano. 2011; 5:42–57. [PubMed: 21182259]
27. Chromy BA, Arroyo E, Blanchette CD, Bench G, Benner H, Cappuccio JA, Coleman MA, Hoeprich PD. Different Apolipoproteins Impact Nanolipoprotein Particle Formation. J Am Chem Soc. 2007; 129:14348–14354. [PubMed: 17963384]
28. Bayburt TH, Sligar SG. Membrane Protein Assembly into Nanodiscs. FEBS letters. 2010; 584:1721–1727. [PubMed: 19836392]
29. Denisov IG, Grinkova YV, Lazarides AA, Sligar SG. Directed Self-Assembly of Monodisperse Phospholipid Bilayer Nanodiscs with Controlled Size. J Am Chem Soc. 2004; 126:3477–3487. [PubMed: 15025475]
30. Pack DW, Chen G, Maloney KM, Chen CT, Arnold FH. A Metal-Chelating Lipid for 2d Protein Crystallization via Coordination of Surface Histidines. J Am Chem Soc. 1997; 119:2479–2487.
31. Zeno WF, Hilt SL, Aravagiri KA, Risbud SH, Voss JC, Parikh AN, Longo ML. Analysis of Lipid Phase Behavior and Protein Conformational Changes in Nanolipoprotein Particles upon Entrapment in Sol–Gel-Derived Silica. Langmuir. 2014; 30:9780–9788. [PubMed: 25062385]
32. Zeno WF, Hilt SL, Risbud SH, Voss JC, Longo ML. Spectroscopic Characterization of Structural Changes in Membrane Scaffold Proteins Entrapped within Mesoporous Silica Gel Monoliths. ACS Appl Mater Interfaces. 2015; 7:8640–8649. [PubMed: 25849085]
33. Jensen MH, Morris EJ, Simonsen AC. Domain Shapes, Coarsening, and Random Patterns in Ternary Membranes. Langmuir. 2007; 23:8135–8141. [PubMed: 17590026]
34. Israelachvili, JN. Intermolecular and Surface Forces: Revised Third Edition. Academic press; Cambridge, MA: 2011.
35. Ratto TV, Longo ML. Obstructed Diffusion in Phase-Separated Supported Lipid Bilayers: A Combined Atomic Force Microscopy and Fluorescence Recovery after Photobleaching Approach. Biophys J. 2002; 83:3380–3392. [PubMed: 12496105]
36. Przybylo M, Sýkora J, Humpolíčková J, Benda A, Zan A, Hof M. Lipid Diffusion in Giant Unilamellar Vesicles is more than 2 Times Faster than in Supported Phospholipid Bilayers under Identical Conditions. Langmuir. 2006; 22:9096–9099. [PubMed: 17042516]
37. Seu KJ, Pandey AP, Haque F, Proctor EA, Ribbe AE, Hovis JS. Effect of Surface Treatment on Diffusion and Domain Formation in Supported Lipid Bilayers. Biophysical journal. 2007; 92:2445–2450. [PubMed: 17218468]
38. Saffman P, Delbrück M. Brownian Motion in Biological Membranes. Proceedings of the National Academy of Sciences. 1975; 72:3111–3113.
39. Balluffi, RW., Allen, S., Carter, WC. Kinetics of Materials. John Wiley & Sons; Hoboken, NJ: 2005.

40. Heberle FA, Wu J, Goh SL, Petruzielo RS, Feigenson GW. Comparison of Three Ternary Lipid Bilayer Mixtures: FRET and ESR Reveal Nanodomains. Biophys J. 2010; 99:3309–3318. [PubMed: 21081079]

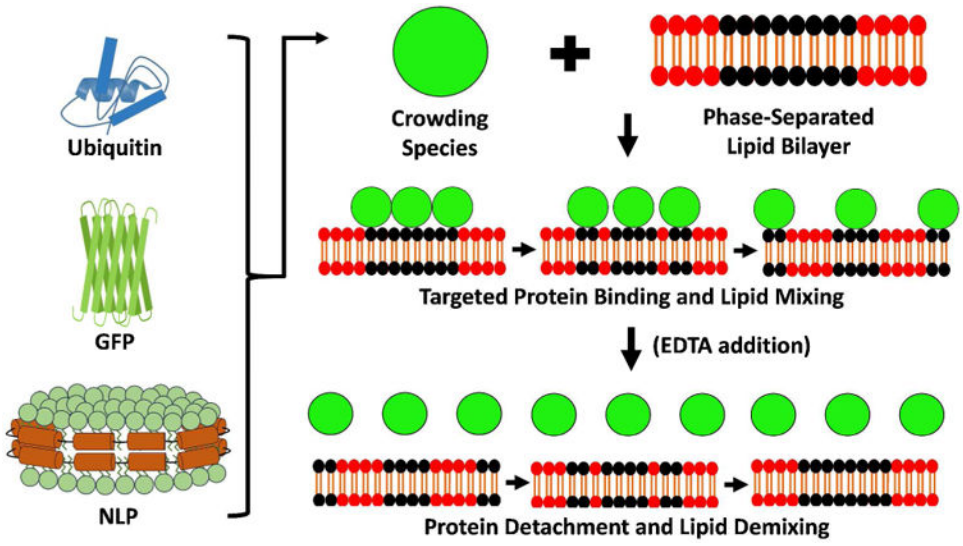


**Figure 1.**

Schematic of crowding-induced mixing in phase-separated lipid bilayers. In this depiction, the $L_o$ phase (black lipids) is targeted by histidine-tagged crowding species that consist of either Ubiquitin, GFP, or NLPs. After removal of these crowding species via EDTA, distinct, separated $L_o$ (black lipids) and $L_d$ (red lipids) phases reappear.

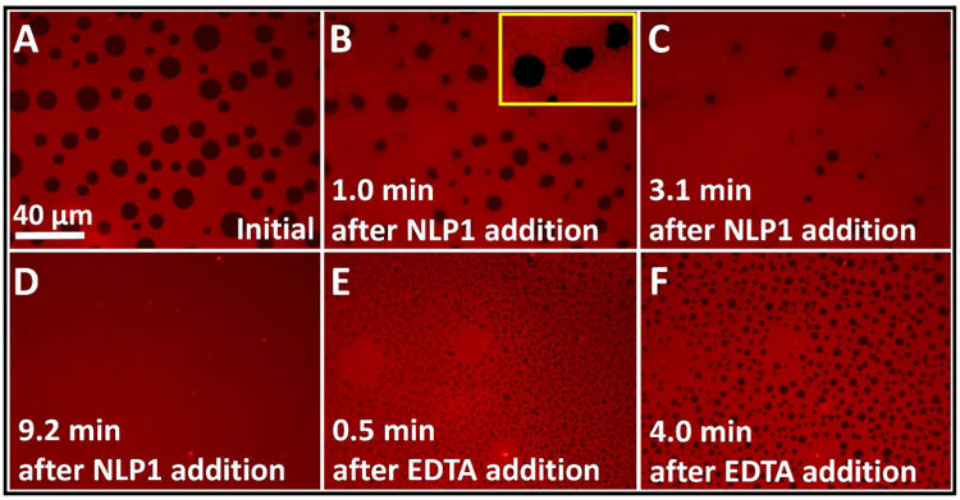


**Figure 2.**

Dissolution of $L_o$ phase domains in $L_o$-$L_d$ phase separated lipid multibilayer after addition of histidine-tagged NLP1 (A-D), followed by removal of NLP1 with EDTA and $L_o$ phase domain reappearance (E & F). Enhanced visualization of graininess surrounding $L_o$ domains is shown in (B) inset. The multibilayer composition was 49.9/20/12/18/0.1 mol% DOPC/DPPC/DPIDA/Cholesterol/Texas Red-DHPE.

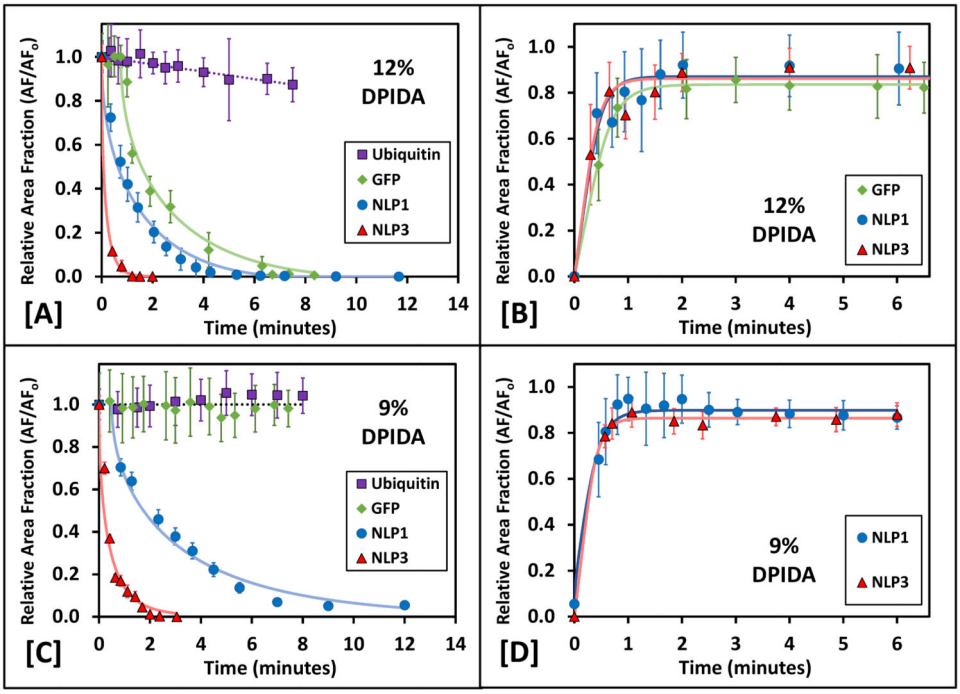


**Figure 3.**

Changes in relative $L_o$ domain area fraction with time after protein addition (A & C) and protein removal with EDTA (B & D) for lipid multibilayer containing different amounts of DPIDA. Corresponding best fit curves to equations 4 and 5 are included. The multibilayer composition was 49.9/32/18/0.1 mol% DOPC/(DPPC+DPIDA)/Cholesterol/Texas Red-DHPE. Error bars are the propagated standard deviation of 4 different area fraction measurements.

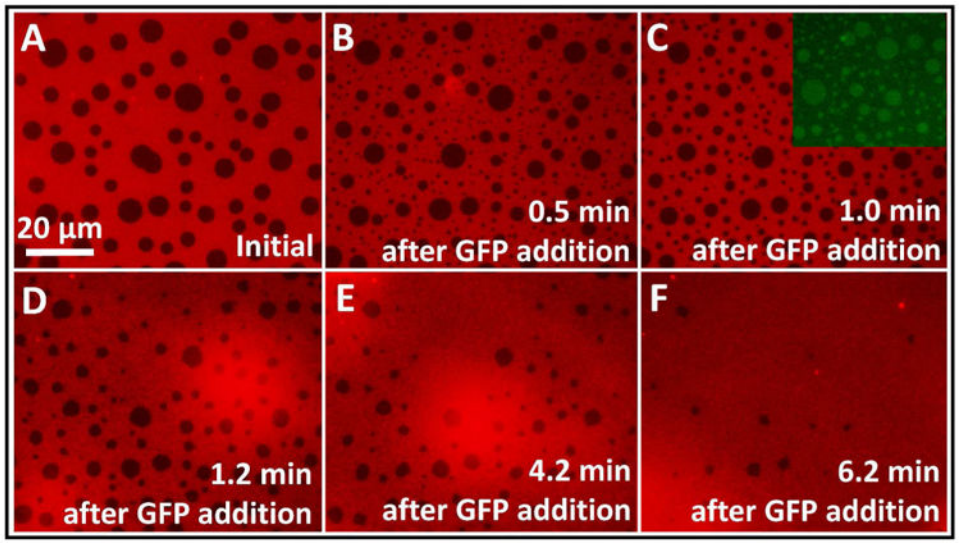


**Figure 4.**

Break-up by ejection of small $L_o$ phase domains in $L_o$-$L_d$ phase separated lipid multibilayer after addition of histidine-tagged GFP (A-B) followed by and coalescence/Ostwald ripening (B-C) and dissolution of the $L_o$ phase domains (D-F). The inset in (C) depicts protein binding visualized via the FITC filter. The multibilayer composition was 49.9/20/12/18/0.1 mol% DOPC/DPPC/DPIDA/Cholesterol/Texas Red-DHPE.

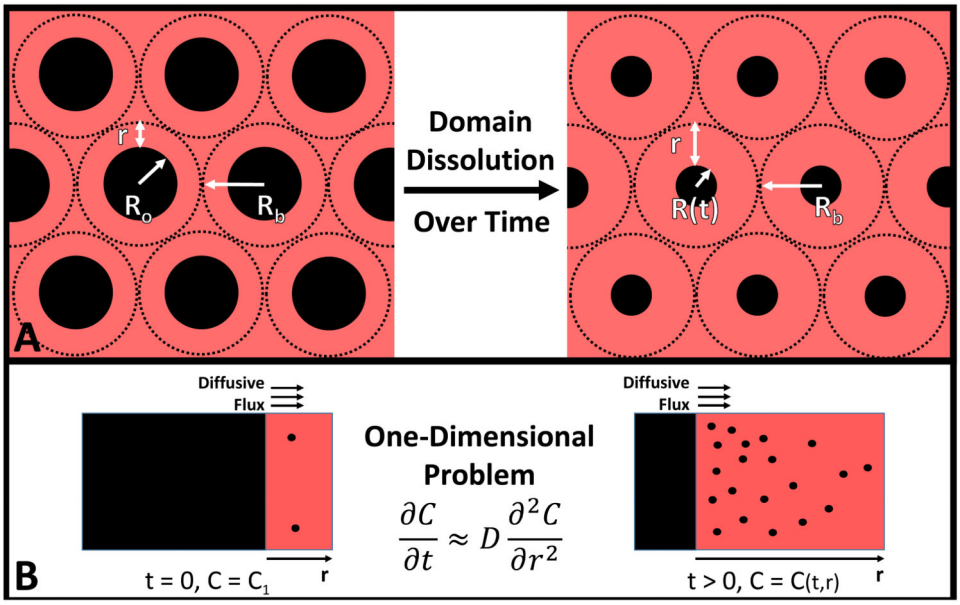


**Figure 5.**

Schematic of idealized liquid ordered phase domain dissolution used in model. At initial time, domains have an average radius of $R_o$. As time progresses, average domain radius R(t) decreases. Diffusion occurs in an annular region with average thickness of r increasing with time (A). The one-dimensional, Cartesian approximation to this problem utilizes a sufficiently thin slice such that the phase boundary is essentially flat (B).

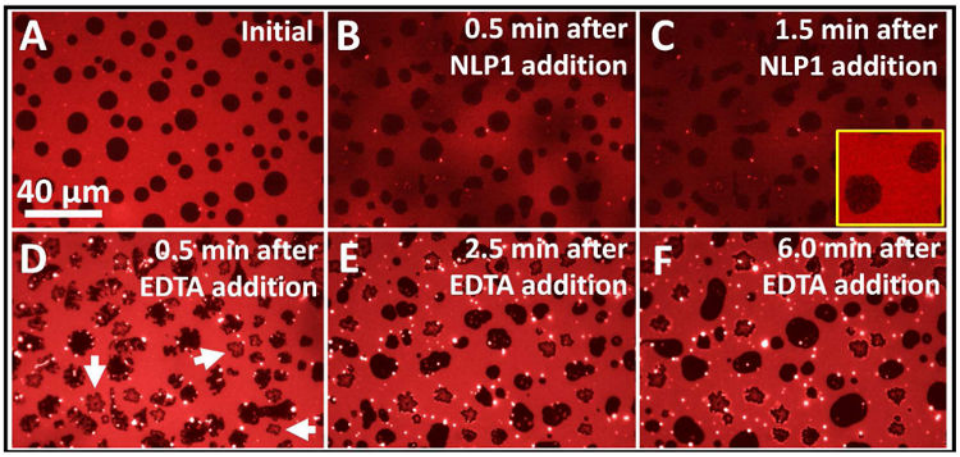


**Figure 6.**

Morphological changes in $L_o$-$L_d$ phase separated lipid multibilayer after addition of histidine-tagged NLP1 (A-C) followed by removal of NLP1 with EDTA that resulted in domain coalescence (D-F). Holes in the bilayer appear as dark red leafy figures (arrows). Enhanced visualization of $L_d$ domains within $L_o$ domains is depicted in (C) inset. The multibilayer composition was 29.9/32/20/18/0.1 mol% DOPC/DPPC/DOIDA/Cholesterol/ Texas Red-DHPE.

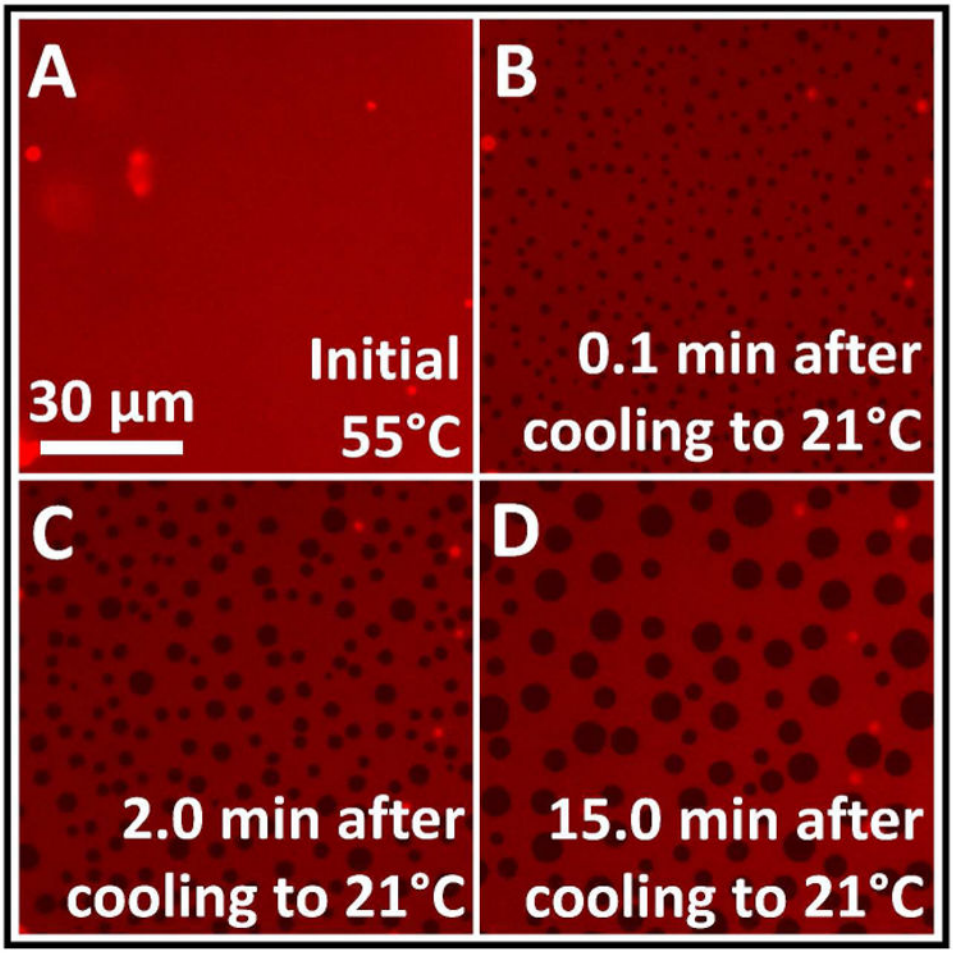


**Figure 7.**
Nucleation and growth observed in MBLs containing 29.9/32/20/18/0.1 mol% DOPC/DPPC/DOIDA/Cholesterol/Texas Red-DHPE.

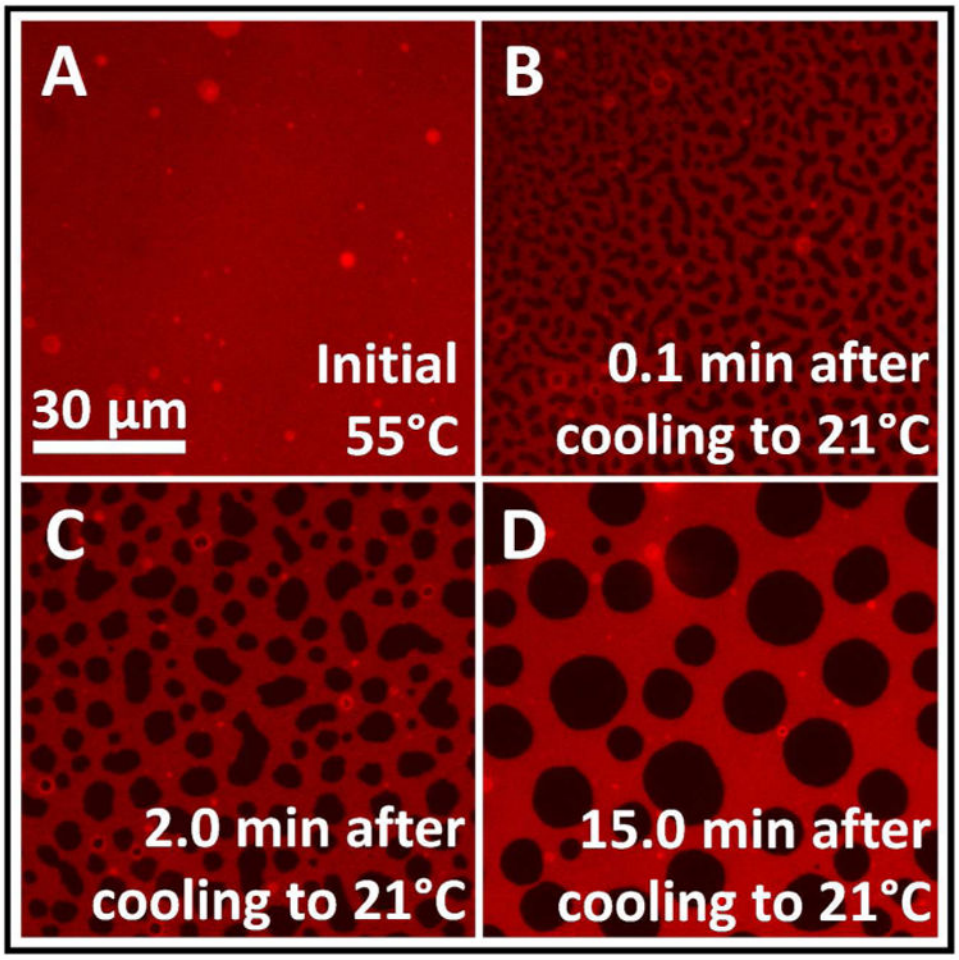


**Figure 8.**
Formation of domains in the spinodal region of the phase diagram with MBLs containing 36.9/23/14/26/0.1 mol% DOPC/DPPC/DPIDA/Cholesterol/Texas Red-DHPE.

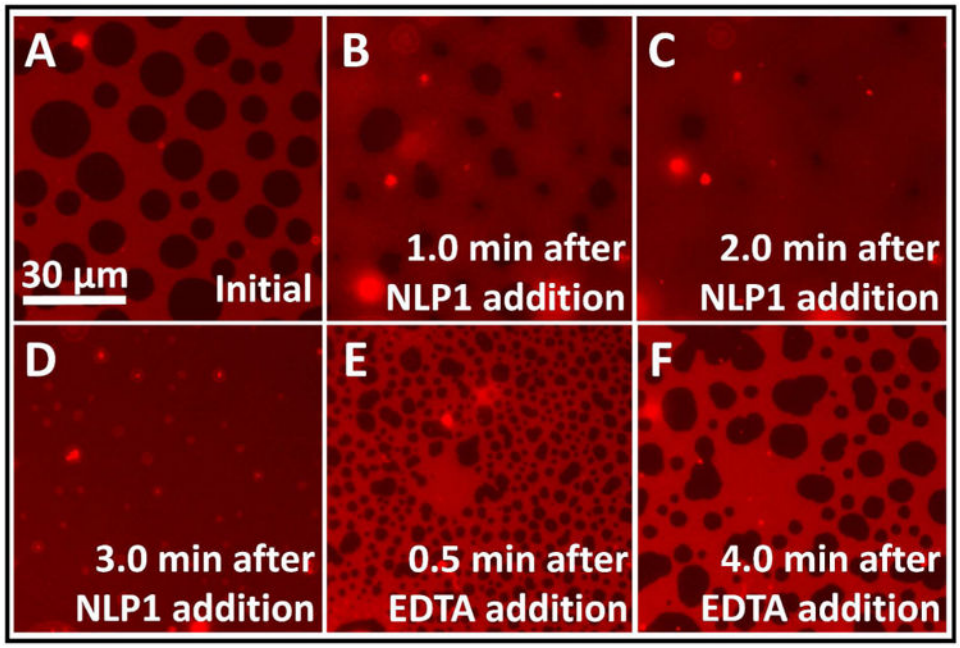


**Figure 9.**

Dissolution of $L_o$ domains by addition of NLP1 to $L_o$-$L_d$ phase separated lipid multibilayer (A-D) and reappearance of domains by spinodal decomposition after addition of 2 mM EDTA (E-F). MBLs contained 36.9/23/14/26/0.1 mol% DOPC/DPPC/DPIDA/Cholesterol/ Texas Red-DHPE.

## Table 1

Regressed values for diffusion coefficients (D) using equations 4 and 5.

| | Crowding Particle | Mixing Diffusion Coefficient (D) ($\mu m^2/s$) | Demixing Diffusion Coefficient (D) ($\mu m^2/s$) |
|---|---|---|---|
| **12% DPIDA** | Ubiquitin | - | - |
| | GFP | 0.02 ± 0.01 | 0.15 ± 0.06 |
| | NLP1 | 0.06 ± 0.01 | 0.55 ± 0.20 |
| | NLP3 | 0.79 ± 0.08 | 0.65 ± 0.22 |
| **9% DPIDA** | Ubiquitin | - | - |
| | GFP | - | - |
| | NLP1 | 0.06 ± 0.01 | 0.62 ± 0.13 |
| | NLP3 | 0.18 ± 0.05 | 0.55 ± 0.11 |